Light-scattering study of dynamical behavior of antiferromagnetic spins in the layered magnetic semiconductor $FePS_3$

T. Sekine,* M. Jouanne, C. Julien, and M. Balkanski
Laboratoire de Physique des Solides, Université Pierre et Marie Curie, 4 place Jussieu, 75252 Paris CEDEX 05, France
(Received 19 March 1990)

Critical phenomena were studied by Raman scattering in the two-dimensional Ising-type antiferromagnet $FePS_3$. Below $T_N = 118$ K the Brillouin-zone-boundary phonon Raman peaks were observed because of the formation of a magnetic superstructure. Above and below T_N a low-frequency broad band was observed, and it was interpreted in terms of Raman scattering from transverse acoustic (TA) phonons throughout the Brillouin zone, which was induced by the spin disorder. The spectrum reflects the two-dimensional one-phonon density of states of the TA phonons. The temperature dependence of the Raman intensity shows a maximum at T_N and agrees with the Ornstein-Zernike form. A quasielastic component due to the magnetic critical scattering was first observed by light scattering. The intensity tends to diverge at T_N. As soon as the spin-disorder-induced Raman spectrum was quenched with decreasing temperature, a one-magnon Raman spectrum began to emerge. The Raman process was discussed using a phenomenological spin-dependent Raman theory.

I. INTRODUCTION

Recently considerable attention has been directed towards the two-dimensional (2D) antiferromagnetic system, because the spin fluctuations are expected to be strong. Interesting problems about the critical phenomena prompted us to study light scattering in 2D antiferromagnets.

Iron phosphorus trisulfide is well known as a 2D Ising-type antiferromagnet. It also has a layered crystal structure with the monoclinic symmetry of space group $C2/m$ (C_{2h}^3),[1] as shown in Fig. 1. The interlayer magnetic interaction is thought to be much smaller than the intralayer magnetic interactions, as well as large anisotropies in lattice dynamics and electronic properties.

A 2D antiferromagnetic ordering occurs at $T_N = 118$ K in the layer.[2] In the antiferromagnetic phase each Fe^{2+} ion, which is arranged in a honeycomb lattice in the paramagnetic phase, is ferromagnetically coupled in a layer with two of the three nearest neighbors. And the ions construct ferromagnetic linear chains which are coupled with each other antiferromagnetically in a layer. The successive layers in the c direction have an antiferromagnetic spin ordering, forming a magnetic superstructure, doubled with respect to the primitive unit cell along the c axis, as well as the $\mathbf{t}_2^*$ axis (see Fig. 2).

Since the critical phenomena have been discovered in the magnetic scattering of neutrons, a number of neutron-scattering experiments and theoretical studies have dealt with the dynamical behaviors of ferromagnetic and antiferromagnetic spins.[3,4] On the other hand, Raman scattering has played an important role in the observation of magnons, which indirectly reflects spin fluctuations in the ordered state. In particular, two-magnon Raman scattering in antiferromagnets yields information on the magnon-magnon interaction, because its spectrum

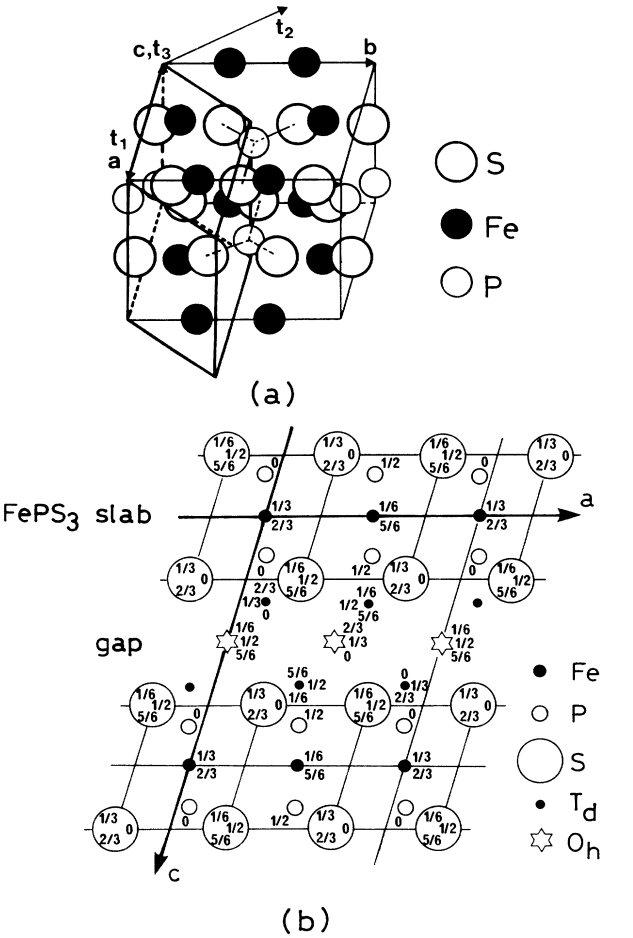

FIG. 1. (a) Crystal structures of $FePS_3$ and (b) its projection along the b axis (from Ref. 1). The thick lines denote the primitive unit cell and $\mathbf{t}_1$, $\mathbf{t}_2$, and $\mathbf{t}_3$ are unit vectors of the primitive unit cell in (a).

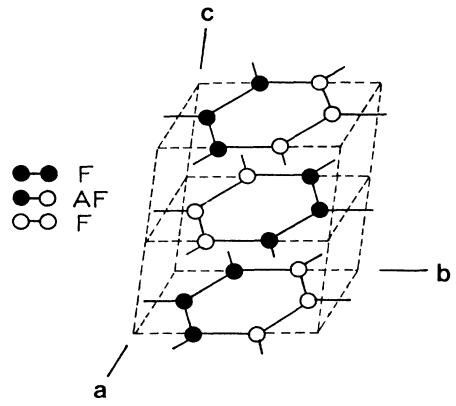

FIG. 2. Magnetic structure of $FePS_3$ presented by Fe atoms. Closed and open circles are up and down atomic spins, respectively (from Ref. 1).

could not be understood within the framework of a simple theory of noninteracting magnons. Hence there has been great interest in the Raman scattering by one magnon and two magnons.[5,6]

Furthermore spin-dependent phonon Raman scattering has been discovered in the ferromagnetic semiconducting spinels $CdCr_2S_4$ and $CdCr_2Se_4$ by Steigmeier and Harbeke.[7] They found that the integrated Raman intensities of certain lines among the Raman-active phonons increase abruptly below the Curie temperature. This has posed new and interesting theoretical problems and has been investigated experimentally and theoretically in magnetic semiconductors, in particular, in the ferromagnetic spinels $CdCr_2S_4$, $CdCr_2Se_4$, and $HgCr_2Se_4$ and in europium chalcogenides EuX (X=O,S,Se,Te). Suzuki and Kamimura[8] proposed a mechanism of the d-electron–phonon scattering process. However, the measurements of Raman scattering of the ferromagnetic spinels with various wavelengths of excitating laser light showed that the increase of the integrated Raman intensity below the Curie temperature is due to the resonant enhancement,[9–11] in addition to the magnetic ordering effect.[12] It occurs when the energy of the excitation light corresponds to that of electronic transition undergoing exchange splitting.

On the other hand, the spin-dependent Raman scattering from the symmetry-forbidden phonons whose spectrum reflects one-phonon density of states has been observed in the paramagnetic phase of the europium chalcogenides. This problem is reviewed in Refs. 13–15. The Raman spectrum shows a broad spectral line of half-width ~ 35 cm^{-1} extending approximately from the Brillouin-zone-center TO-phonon to the LO-phonon frequencies. Tsang *et al.*[16] pointed out that it originated from a symmetry-breaking mechanism due to spin disorder. When the spins are randomly aligned, the spin disorder lifts the inversion and translational symmetry in the phonon-plus-spin system, which allows us to observe the first-order Raman scattering from phonons with finite wave vectors.

As the long-range magnetic ordering is induced by reducing temperature through the transition temperature and by applying the magnetic field, the broad bands due to the spin-disorder-induced Raman scattering are rapidly quenched, and new sharp lines appear in EuSe (Refs. 14 and 17–20) and EuTe.[18,21] The appearance of first-order Raman scattering originates from the Brillouin-zone-folding effect due to the formation of magnetic superstructure, i.e., it is attributed to inelastic scattering from the zone-boundary phonons and the mid-zone phonons induced by the elastic ("Bragg") magnetic scattering from the magnetic superstructure.[13,14,22–24] Similarly the zone-boundary phonons were observed in the antiferromagnetic phase of VI_2.[25]

On the other hand, Silberstein *et al.*[19] observed that the broad line due to the spin-disorder-induced Raman scattering is continuously switched to a sharp line upon cooling from the paramagnetic phase to the ferromagnetic phase in EuS. Güntherodt *et al.*[26] found that the peak positions of the broad bands shift continuously to the high-frequency side in the ferromagnetic phases of EuS and EuO. The frequency shifts are unusually large for phonons only. Güntherodt *et al.*[26] and Silberstein[20] explained them by switching from the spin-disorder-induced Raman scattering to the second-order process of one magnon plus one phonon upon cooling through the ordering temperature. The frequency shifts result from the frequencies of magnons.

Recently the effect of magnetic ordering on the phonon Raman scattering has been studied in another class of layered compounds, the transition-metal phosphorous trichalcogenides MPX_3 (M=transition metal, X=S,Se).[27–29] The enhancement of Raman intensities of Raman-active phonon peaks and the appearance of new phonons have been observed below T_N in the Raman spectra of $FePS_3$.

In this paper we shall focus on the effect of spin fluctuations on the Raman spectra of the 2D antiferromagnet $FePS_3$ and study the critical pheneomena in the antiferromagnetic phase transition. We observe the low-frequency Raman scattering from transverse acoustic (TA) phonons with finite wave vectors which are induced by spin disorder in the paramagnetic and the antiferromagnetic-ordered states. In the vicinity of the Néel temperature we found strong enhancement of the quasielastic component in the low-frequency Raman spectrum. It is due to the magnetic critical scattering by light. To the best of our knowledge, this is the first report of this kind. In the temperature region where the spin-disorder-induced Raman spectrum is quenched, we observe Raman scattering from a magnon. We shall discuss their effects of spin fluctuations and spin ordering on the Raman scattering by a phenomenological theory.

II. EXPERIMENTAL

The single crystals of $FePS_3$ used were synthesized by the vapor-transport method. The surfaces with good optical quality were easily obtained by cleaving.

The Raman-scattering measurements were performed with use of the argon-ion laser lines in a quasibackscatter-

ing geometry with the Brewster-angle incidence. To avoid sample heating by the laser beam only few tens of milliwatts were used in the present experiment. Measurements were carried out as a function of the temperature by employing a variable-temperature SMC-TBT cryostat. The scattered light was dispersed with an instrumental resolution of about 1.5 cm^{-1} by a double-grating monochromator Jobin-Yvon U1000 with holographic gratings and detected by a photon-counting system.

III. RESULTS

Figure 3 shows the temperature dependence of the low-frequency anti-Stokes and Stokes Raman spectra in the $z(x, x+y)\bar{z}$ geometry in $FePS_3$. Here z is perpendicular to the basal plane or parallel to the t_3^* (c^*), and x and y denote two arbitrary, but mutually perpendicular, directions on the basal plane. Since the refractive index is large, the wave vector of the incident light is approximately perpendicular to the surface within the sample. In the paramagnetic state we observed an asymmetric peak at about 100 cm^{-1} with a low-frequency tail. It has a very steep slope at the high-frequency side. As the frequency shift is decreased below about 60 cm^{-1}, so does the Raman intensity. We can also see this structure below $T_N = 118$ K, but cannot see it below 85 K, which is far below T_N, except for the low-frequency component. This quasielastic component is due to the magnetic critical scattering, as will be discussed below. The asymmetric peak at about 100 cm^{-1} and the quasielastic scattering show a maximum in Raman intensity and disappear almost completely at 21 K.

Below $T_N = 118$ K four new sharp peaks appear at 88, 94, 108, and 122 cm^{-1}. Figure 4 shows the temperature dependence of the Stokes Raman spectrum. The frequency of the 122-cm^{-1} (21-K) peak shifts to the low-frequency side with increasing temperature, while the frequencies of the other three peaks remain unchanged. The former is a Raman peak from a magnon, as will be discussed later.

The Stokes Raman spectrum may be described by a spectral function,

$$I(\omega)=\frac{K^2}{\pi}[n(\omega)+1]\frac{\Gamma}{(\omega-\omega_0)^2+\Gamma^2}+b_g\ , \tag{1}$$

where ω_0, Γ, and K are the phonon frequency, the damping constant, and the coupling coefficient of the phonon for the photon, respectively. $n(\omega)$ is the Bose factor, and b_g is the background. The integrated intensity is given as

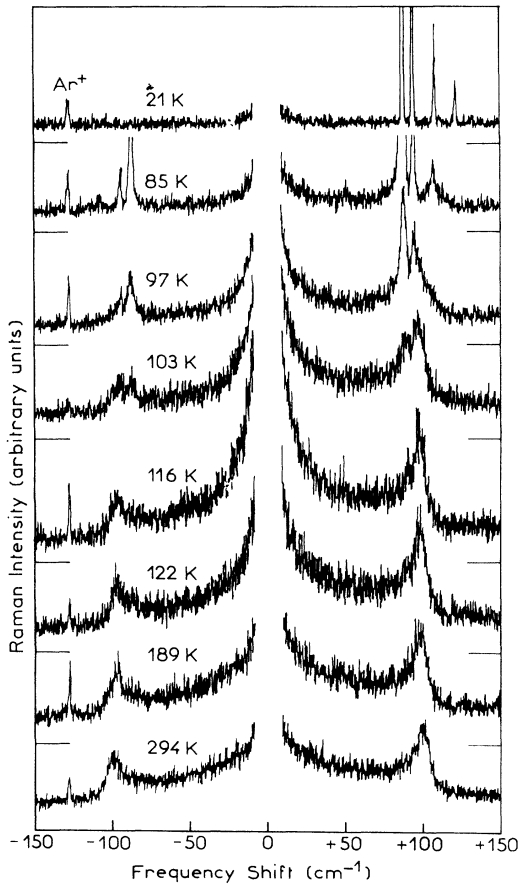

FIG. 3. Temperature dependence of Stokes and anti-Stokes Raman spectra in $FePS_3$. Ar^+ means a plasma line of an Ar^+ laser.

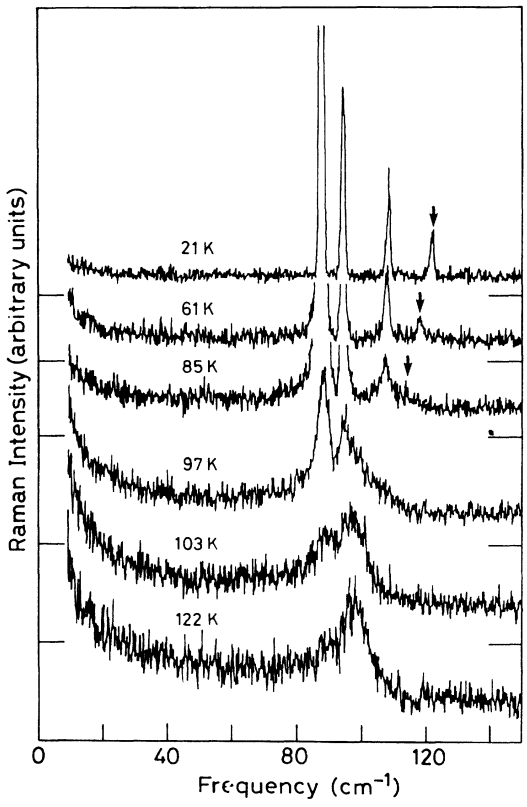

FIG. 4. Temperature dependence of Stokes Raman spectrum at low temperatures in $FePS_3$. Arrows show the one-magnon Raman peaks.

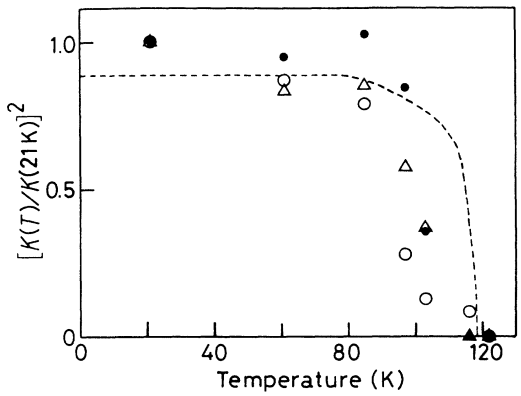

FIG. 5. Normalized square of the coupling coefficients K^2 of phonon peaks at 88 (○), 94 (△), and 108 (●) cm^{-1}. A dotted curve denotes the square of the magnetic moment of Fe^{2+} ion obtained by neutron diffraction (Ref. 2).

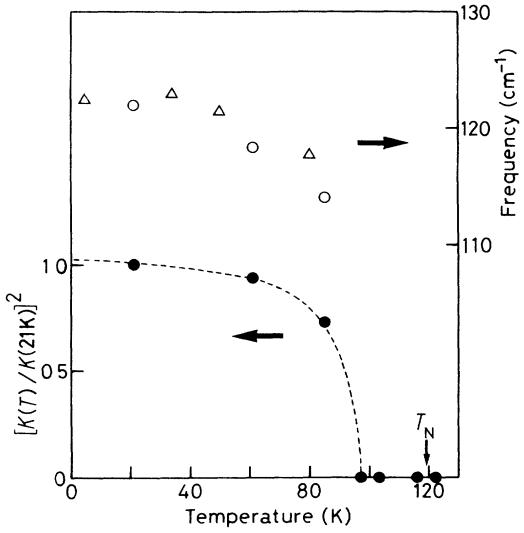

FIG. 6. Temperature dependence of the frequency ω_0 and of the square of coupling coefficient K^2 of the 122-cm^{-1} (21-K) peak. Triangles were obtained by infrared absorption. A dotted curve is only guide for the eye.

$$\int_{-\infty}^{+\infty} d\omega[I(\omega)-b_g]\sim K^2[n(\omega_0)+1]\ . \tag{2}$$

The obtained squares of the coupling constants for the peaks at 88, 94, and 108 cm^{-1} are shown in Fig. 5. The frequency and the square of the coupling constant of the 122-cm^{-1} peak as a function of the temperature are shown Fig. 6, in addition to the frequency obtained by infrared-absorption measurements.

IV. THEORY OF THE SPIN-DEPENDENT PHONON RAMAN SCATTERING

The spin-dependent Raman scattering from phonons has been discussed theoretically by many authors.[8,13,14,22–24,26,30–32] We shall develop theoretical discussion about the spin-dependent phonon Raman scattering in terms of the phenomenological theory.[8,13,26,30,33] The Raman scattering $I(\omega)$ is related to the electronic susceptibility as follows:

$$I(\omega)=\frac{\omega_i^4}{2\pi c^3}\sum_{a,b,a',b'} E_a^s E_{b'}^s E_b^i E_{a'}^i \frac{1}{2\pi}\int_{-\infty}^{+\infty} dt\, e^{-i\omega t}\langle \chi_{b'a}(t)\chi^*_{a'b}(0)\rangle\ , \tag{3}$$

where E_a^i (E_a^s) is the polarization vector component of the incident (scattered) photon, $\omega=\omega_i-\omega_s$, ω_i (ω_s) is the frequency of the incident (scattered) light, c is the light velocity, the bracket $\langle\ \rangle$ denotes the canonical ensemble average, and

$$\chi_{b'a}(t)=e^{i(t/\hbar)H}\chi_{b'a}e^{-i(t/\hbar)H}\ . \tag{4}$$

Here H is the Hamiltonian. In order to describe the spin-dependent Raman scattering, the electronic susceptibility may be expanded in powers of the displacements of the ions from their equilibrium and of the ion spins:[8,13,26,30,33]

$$\begin{aligned}\chi_{ab}=&\chi^0_{ab}+\sum\chi_{ab}(j;\kappa,s)u_j(\kappa,s)+\sum\chi_{ab}(j;\kappa,s;j';\kappa',s')u_j(\kappa,s)u_{j'}(\kappa',s')+\sum\chi_{ab}(\sigma;\tau,m)S_\sigma(\tau,m)\\&+\sum\chi_{ab}(\sigma;\tau,m;\sigma';\tau',m')S_\sigma(\tau,m)S_{\sigma'}(\tau',m')+\sum\chi_{ab}(j;\kappa,s;\sigma;\tau,m)u_j(\kappa,s)S_\sigma(\tau,m)\\&+\sum\chi_{ab}(j;\kappa,s;\sigma;\tau,m;\sigma';\tau',m')u_j(\kappa,s)S_\sigma(\tau,m)S_{\sigma'}(\tau',m')+\cdots\ .\end{aligned} \tag{5}$$

Here

$$\chi_{ab}(j;\kappa,s)=\frac{\partial\chi_{ab}}{\partial u_j(\kappa,s)}\ , \tag{6a}$$

$$\chi_{ab}(j;\kappa,s;j';\kappa',s')=\frac{\partial^2\chi_{ab}}{\partial u_j(\kappa,s)\partial u_{j'}(\kappa',s')}\ , \tag{6b}$$

$$\chi_{ab}(\sigma;\tau,m)=\frac{\partial\chi_{ab}}{\partial S_\sigma(\tau,m)}\ , \tag{6c}$$

$$\chi_{ab}(\sigma;\tau,m;\sigma';\tau',m')=\frac{\partial^2\chi_{ab}}{\partial S_\sigma(\tau,m)\partial S_{\sigma'}(\tau',m')}\ , \tag{6d}$$

$$\chi_{ab}(j;\kappa,s;\sigma;\tau,m)=\frac{\partial^2\chi_{ab}}{\partial u_j(\kappa,s)\partial S_\sigma(\tau,m)}\ , \tag{6e}$$

$$\chi_{ab}(j;\kappa,s;\sigma;\tau,m;\sigma';\tau',m') = \frac{\partial^3 \chi_{ab}}{\partial u_j(\kappa,s)\partial S_\sigma(\tau,m)\partial S_{\sigma'}(\tau',m')} , \quad (6f)$$

$u_j(\kappa,s)$ is the jth component of the displacement of the sth nonmagnetic or magnetic ion in the κth unit cell, $S_\sigma(\tau,m)$ is the σ component of the mth magnetic ion spin in the τth unit cell, and $j,\sigma=(x,y,z)$.

The second and third terms in Eq. (5) represent the first- and second-order Raman scattering from phonons, respectively. The fourth and fifth terms show the first- and second-order Raman scattering from magnons below T_N, respectively. The sixth and seventh terms give rise to Raman scattering under simultaneous excitations of the phonon and spin systems linear and quadratic in the spins, respectively. The displacement is given by

$$u_j(\kappa,s)=\sum_{\mathbf{q},n}\left[\frac{\hbar}{2NM_s\omega_n(\mathbf{q})}\right]^{1/2}\varepsilon_{nj}(s,\mathbf{q}) \times e^{-i\mathbf{q}\cdot\mathbf{R}(\kappa)}[\alpha_n(\mathbf{q})+\alpha_n^\dagger(-\mathbf{q})] , \quad (7)$$

where N is the number of unit cells in the crystal, M_s is the mass of the sth ion, $\mathbf{R}(\kappa)$ is the position vector of the κth unit cell, and $\alpha_n(\mathbf{q})$ [$\alpha_n^\dagger(\mathbf{q})$] is the annihilation (creation) operator of the normal mode of branch n with frequency $\omega_n(\mathbf{q})$, wave vector $\mathbf{q}$, and jth component of the polarization vector $\varepsilon_{nj}(s,\mathbf{q})$. Similarly we get

$$S_\sigma(\tau,m)=N^{-1/2}\sum_{\mathbf{q}} S_{m\sigma}(\mathbf{q})e^{-i\mathbf{q}\cdot\mathbf{R}(\tau)} . \quad (8)$$

Several authors[13,14,19,20,22–24,26,34] pointed out that the spin-disorder- and the spin-ordering-induced phonon Raman scattering can be interpreted in terms of one-spin–one-phonon mechanism. The sixth term is the most important in Eq. (5) and takes an essential role in the spin-dependent phonon Raman scattering in magnetic semiconductors. We, therefore, take only the sixth term into account. The interaction between the displacement of the ion and the ion spin originates from the electron-phonon interaction and from the spin-orbit interaction which couples the electron angular momentum to the localized spin. Substituting Eqs. (7) and (8) into Eq. (5), we obtain

$$\chi_{ab}(j;\kappa,s;\sigma;\tau,m)u_j(\kappa,s)S_\sigma(\tau,m)=\sum_{\mathbf{q},n}\chi_{ab}(j,s;\sigma,m;\mathbf{q})\left[\frac{N\hbar}{2M_s\omega_n(\mathbf{q})}\right]^{1/2}\varepsilon_{nj}(s,\mathbf{q})A_n(\mathbf{q})S_{m\sigma}(-\mathbf{q}) , \quad (9)$$

where $A_n(\mathbf{q})=\alpha_n(\mathbf{q})+\alpha_n^\dagger(-\mathbf{q})$ and $\chi_{ab}(j,s;\sigma,m;\mathbf{q})$ is a Fourier component of $\chi_{ab}(j;\kappa,s;\sigma;\tau,m)$ since it depends on the vectors $\mathbf{R}(\kappa)$ and $\mathbf{R}(\tau)$ only through their difference $\mathbf{R}(p)=\mathbf{R}(\kappa)-\mathbf{R}(\tau)$, i.e.,

$$\chi_{ab}(j;\kappa,s;\sigma;\tau,m)=N^{-1/2}\sum_{\mathbf{q}}\chi_{ab}(j,s;\sigma,m;\mathbf{q})e^{-i\mathbf{q}\cdot\mathbf{R}(p)} . \quad (10)$$

Using Eq. (9), the Raman spectrum may be rewritten as

$$I(\omega)=\frac{\omega_i^4}{2\pi c^3}\sum_{a,b,a',b'}E_{a'}^s E_{b'}^s E_b^i E_a^i\sum\chi_{b'a}(j,s;\sigma,m;\mathbf{q})\chi_{a'b}^*(j',s';\sigma',m';\mathbf{q}) \times\left[\frac{N\hbar}{2}\right]\left[\frac{1}{M_sM_{s'}\omega_n(\mathbf{q})\omega_{n'}(\mathbf{q})}\right]^{1/2}\varepsilon_{nj}(s,\mathbf{q})\varepsilon_{n'j'}^*(s',\mathbf{q}) \times\frac{1}{2\pi}\int_{-\infty}^{+\infty}dt\,e^{-i\omega t}\langle A_n(\mathbf{q};t)A_{n'}^\dagger(\mathbf{q};0)\rangle\langle S_{m\sigma}(-\mathbf{q};t)S_{m'\sigma'}^*(-\mathbf{q};0)\rangle . \quad (11)$$

Here we have used the relation[35]

$$\langle A_n(\mathbf{q};t)A_{n'}^\dagger(\mathbf{q}';0)\rangle=\delta(\mathbf{q}-\mathbf{q}')\langle A_n(\mathbf{q};t)A_{n'}^\dagger(\mathbf{q};0)\rangle . \quad (12)$$

In the temperature region where the magnon picture does not hold, spin correlation is approximately independent of ω or the time t and represented as[3,13]

$$\sum_{\sigma,\sigma'}\langle S_{m\sigma}(-\mathbf{q};t)S_{m'\sigma'}^*(-\mathbf{q};0)\rangle\sim\langle S_{mz}(-\mathbf{q})\rangle\langle S_{m'z}(\mathbf{q})\rangle\delta(\mathbf{q}-\mathbf{t}_2^*/2)+\sum_{\sigma,\sigma'}\langle\tilde{S}_{m\sigma}(-\mathbf{q})\tilde{S}_{m'\sigma'}(\mathbf{q})\rangle\delta_{\sigma\sigma'} . \quad (13)$$

Here

$$\tilde{S}_{m\sigma}(-\mathbf{q};t)=S_{m\sigma}(-\mathbf{q};t)-\langle S_{m\sigma}(-\mathbf{q})\rangle , \quad (14)$$

which represents the spin fluctuations. Below T_N, $\langle S_{mz}(\mathbf{q})\rangle$ appears at $\mathbf{q}=\mathbf{t}_2^*/2$ and the magnetic structure becomes doubled with respect to the primitive lattice unit cell, as shown in Fig. 2 and as will be discussed later.

Using the Green's function $G(\mathbf{q};n,n';\omega)$ for phonon,[35]

$$G(\mathbf{q},n,n';i\omega_l)=\beta^{-1}\int_0^\beta du\langle\mathcal{T}A_n(\mathbf{q};u)A_{n'}^\dagger(\mathbf{q};0)\rangle e^{-\beta\omega_l u} , \quad (15)$$

where $\mathcal{T}$ is the time ordering operator, $u=it/\hbar$, $\beta=1/k_BT$, and $\omega_l=2\pi l/(\beta\hbar)$, and taking the lattice anharmonicity into account, the phonon correlation function is given as follows:[35]

$$\int_{-\infty}^{+\infty} dt\, e^{-i\omega t}\langle A_n(\mathbf{q};t)A_{n'}^{\dagger}(\mathbf{q};0)\rangle = \frac{2\pi\beta\hbar}{1-e^{-\beta\hbar\omega}} \lim_{\delta\to 0+} \frac{G(\mathbf{q},n,n';\omega+i\delta)-G(\mathbf{q},n,n';\omega-i\delta)}{2\pi i}$$

$$\sim \delta_{nn'} \frac{1}{i(1-e^{-\beta\hbar\omega})} \lim_{\delta\to 0+} \left[\frac{1}{\omega+i\delta+\omega_n(\mathbf{q})-\mathscr{g}(\mathbf{q},n;\omega+i\delta)/\beta\hbar} - \frac{1}{\omega-i\delta+\omega_n(\mathbf{q})-\mathscr{g}(\mathbf{q},n;\omega-i\delta)/\beta\hbar} + \frac{1}{-\omega-i\delta+\omega_n(\mathbf{q})-\mathscr{g}(\mathbf{q},n;\omega+i\delta)/\beta\hbar} - \frac{1}{-\omega+i\delta+\omega_n(\mathbf{q})-\mathscr{g}(\mathbf{q},n;\omega-i\delta)/\beta\hbar} \right] . \tag{16}$$

Here $\mathscr{g}(\mathbf{q},n;\omega)$ is the self-energy part and is given as[35]

$$\lim_{\delta\to 0+} [-\mathscr{g}(\mathbf{q},n;\omega\pm i\delta)/\beta\hbar] = \Delta_n(\mathbf{q};\omega) \mp i\Gamma_n(\mathbf{q};\omega) . \tag{17}$$

If $\Delta_n(\mathbf{q};\omega)$ and $\Gamma_n(\mathbf{q};\omega)$ are small compared with $\omega_n(\mathbf{q})$, we obtain

$$\int_{-\infty}^{+\infty} dt\, e^{-i\omega t}\langle A_n(\mathbf{q};t)A_{n'}^{\dagger}(\mathbf{q};0)\rangle \sim \delta_{nn'} \frac{2}{1-e^{-\beta\hbar\omega}} \left[\frac{\Gamma_n(\mathbf{q})}{[\omega-\hat{\omega}_n(\mathbf{q})]^2+\Gamma_n^2(\mathbf{q})} - \frac{\Gamma_n(\mathbf{q})}{[\omega+\hat{\omega}_n(\mathbf{q})]^2+\Gamma_n^2(\mathbf{q})} \right] , \tag{18}$$

where $\hat{\omega}_n(\mathbf{q})$ is the renormalized frequency:

$$\hat{\omega}_n(\mathbf{q}) = \omega_n(\mathbf{q}) + \Delta_n(\mathbf{q};\omega) . \tag{19}$$

In arriving at this result, we used the fact that $\Delta_n(\mathbf{q};\omega)$ is an even function of ω, while $\Gamma_n(\mathbf{q};\omega)$ is an odd function of ω and we have set $\Gamma_n(\mathbf{q};+|\omega|) = -\Gamma_n(\mathbf{q};-|\omega|) \sim \Gamma_n(\mathbf{q})$,[35] where $\Gamma_n(\mathbf{q})$ is independent of ω. The first term of the parenthesis in Eq. (18) denotes the Stokes component, and the second term the anti-Stokes one.

V. SPIN-ORDERING-INDUCED PHONON RAMAN SCATTERING

The first term in Eq. (13) gives the Raman scattering for the normal mode of branch n at $q = \mathbf{t}_2^*/2$ which is induced by the spin ordering below T_N:

$$I_n(\omega) = C_n^2(\mathbf{t}_2^*/2) \frac{1}{1-e^{-\beta\hbar\omega}} \frac{1}{\omega(\mathbf{t}_2^*/2)} \frac{1}{\pi} \left[\frac{\Gamma_n(\mathbf{t}_2^*/2)}{[\omega-\hat{\omega}_n(\mathbf{t}_2^*/2)]^2+\Gamma_n^2(\mathbf{t}_2^*/2)} - \frac{\Gamma_n(\mathbf{t}_2^*/2)}{[\omega+\hat{\omega}_n(\mathbf{t}_2^*/2)]^2+\Gamma_n^2(\mathbf{t}_2^*/2)} \right] \times \sum_{m,m'} \langle S_{mz}(-\mathbf{t}_2^*/2)\rangle \langle S_{m'z}(\mathbf{t}_2^*/2)\rangle , \tag{20}$$

where $C_n(\mathbf{q})$ is proportional to the Raman tensor and it is given by

$$C_n^2(\mathbf{q}) = \frac{\omega_i^4}{2\pi c^3} \sum E_a^s E_{b'}^s E_b^i E_{a'}^i \sum \chi_{b'a}(j,s;\sigma,m;\mathbf{q}) \chi_{a'b}^*(j',s';\sigma',m';\mathbf{q}) \left[\frac{N\hbar}{2}\right] \left[\frac{1}{M_s M_{s'}}\right]^{1/2} \varepsilon_{nj}(s,\mathbf{q}) \varepsilon_{nj'}(s',\mathbf{q}) . \tag{21}$$

We assume that it is independent of σ, σ', m, and m', but it depends on the polarization and the frequency of the incident light, and the polarizations of the scattered light and of the normal mode of branch n, although their suffixes are omitted.

Equation (20), therefore, represents the three sharp peaks at 88, 94, and 108 cm^{-1} appearing below T_N. They are Raman-inactive phonons with the zone-boundary wave vector of $\mathbf{q} = \mathbf{t}_2^*/2$ in the paramagnetic phase. The "spin lattice" becomes doubled with respect to the chemical primitive unit cell along the basal layered plane. Then the zone-boundary phonons at $\mathbf{q} = \mathbf{t}_2^*/2$ become Raman active below T_N. Bernasconi *et al.*[36] calculated lattice dynamics of MPX_3, where M = Mn, Fe, Ni or Zn and X = S or Se. The zone-boundary reciprocal-lattice point at $\mathbf{q} = \mathbf{t}_2^*/2$ corresponds to the M point in the Brillouin zone. The 88-cm^{-1} peak can be assigned to acoustic modes at $\mathbf{q} = \mathbf{t}_2^*/2$ in which all atoms vibrate approximately along the basal plane. Their frequencies are almost degenerate. The 94-cm^{-1} peak is assigned to an optical mode, and the 108-cm^{-1} peak to a TA mode in which all atoms vibrate approximately along the z direction, i.e., the $\mathbf{t}_3^*$ or $\mathbf{c}^*$ axis. Scagliotti *et al.*[27,28] have observed the appearance of new peak at 161 cm^{-1} below T_N in addition to the three peaks. It is also assigned to an optical mode at the M point.

The integrated Raman intensity for the Stokes scattering is given as

$$I_n \sim C^2 \{ n[\hat{\omega}_n(\mathbf{t}_2^*/2)]+1 \} \times [\langle S_{1z}(\mathbf{t}_2^*/2)\rangle + \langle S_{2z}(\mathbf{t}_2^*/2)\rangle]^2 , \tag{22}$$

where $C^2=C_n^2(\mathbf{t}_2^*/2)/\omega(\mathbf{t}_2^*/2)$. Comparison between Eqs. (2) and (22) gives

$$K^2\sim C^2[\langle S_{1z}(\mathbf{t}_2^*/2)\rangle+\langle S_{2z}(\mathbf{t}_2^*/2)\rangle]^2 . \tag{23}$$

We obtain that at $T>T_N$

$$\langle S_{1z}(\mathbf{t}_2^*/2)\rangle+\langle S_{2z}(\mathbf{t}_2^*/2)\rangle=0 , \tag{24a}$$

and at $T<T_N$

$$\langle S_{1z}(\mathbf{t}_2^*/2)\rangle+\langle S_{2z}(\mathbf{t}_2^*/2)\rangle\propto M(T) , \tag{24b}$$

where $M(T)$ is the magnetic moment of the Fe^{2+} ion. The dotted curve in Fig. 5 denotes the square of the magnetic moment obtained by neutron diffraction.[2] The agreement is roughly good, but not very good near the Néel temperature. We do not have good explanation for the disagreement near T_N at present.

VI. SPIN-DISORDER-INDUCED PHONON RAMAN SCATTERING

The second term in Eq. (13) describes the phonon Raman scattering which is induced by spin disorder. Marshall and Lowde[3] obtained the Ornstein-Zernike form for the spin correlation function. Taking into consideration that the spin system of $FePS_3$ is described by the Ising model, in the vicinity of T_N, it may be written as

$$\sum_{m,m'}\sum_{\sigma}\langle\tilde{S}_{m\sigma}(-\mathbf{q})\tilde{S}_{m'\sigma}(\mathbf{q})\rangle=\frac{2S(2S+1)}{3}\frac{\chi_{zz}(\mathbf{q})}{\chi_0} , \tag{25}$$

where S is the magnitude of the spin at the Fe^{2+} ion. Using mean-field theory, the magnetic susceptibility is written in the form

$$\frac{\chi_{zz}(\mathbf{q})}{\chi_0}=\frac{\lambda_0^2 T/T_N}{\lambda^2+\lambda_0^2[J(\mathbf{t}_2^*/2)-J(\mathbf{q})]/J(\mathbf{t}_2^*/2)} , \tag{26}$$

where $J(\mathbf{q})$ is the exchange interaction. The inverse correlation length λ is determined in the mean-field theory as

$$\lambda^2=\begin{cases}\lambda_0^2(T/T_N-1), & \text{for } T>T_N \quad (27a)\\ 2\lambda_0^2(1-T/T_N), & \text{for } T<T_N . \quad (27b)\end{cases}$$

Assuming that $\chi_{zz}(\mathbf{q})/\chi_0$ is independent of $\mathbf{q}$ and denoting it by χ_{zz}/χ_0, the Raman scattering for the n-branch mode becomes

$$I_n(\omega)\sim C_n^2(\omega)\frac{2S(2S+1)}{3}\frac{\chi_{zz}}{\chi_0}\frac{1}{1-e^{-\beta\hbar\omega}}\frac{1}{\pi}\sum_{\mathbf{q}}\left[\frac{1}{\hat{\omega}_n(\mathbf{q})}\left[\frac{\Gamma_n(\mathbf{q})}{[\omega-\hat{\omega}_n(\mathbf{q})]^2+\Gamma_n^2(\mathbf{q})}-\frac{\Gamma_n(\mathbf{q})}{[\omega+\hat{\omega}_n(\mathbf{q})]^2+\Gamma_n^2(\mathbf{q})}\right]\right] . \tag{28}$$

Here we replaced $C_n(\mathbf{q})$ by $C_n(\omega)$ which is a function of ω. If $\Gamma_n(\mathbf{q})=0$, we obtain

$$I_n(\omega)\sim C_n^2(\omega)\frac{2S(2S+1)}{3}\frac{\chi_{zz}}{\chi_0}\frac{1}{1-e^{-\beta\hbar\omega}}\frac{D_n(|\omega|)}{\omega} , \tag{29}$$

where $D_n(\omega)$ is the one-phonon density of states of the n-branch mode, i.e., the Raman spectrum reflects the one-phonon density of states.

The low-frequency broad band with an asymmetric peak at about 100 cm^{-1} can be ascribed to the spin-disorder-induced Raman scattering from the TA phonon, in which all atoms vibrate approximately along the z axis, with $q_z=0$ on the basal $\mathbf{t}_3^*$ plane. For simplicity we assume that the dispersion of the TA phonon with $q_r=(q_x^2+q_y^2)^{1/2}$ along the basal plane is written as

$$\hat{\omega}_{\mathrm{TA}}(\mathbf{q})=\omega_m|\sin(q_r r/2)|, \quad \text{for } 0\le q_r\le q_m , \tag{30}$$

where

$$\pi q_m^2=\frac{8\pi^2}{3^{1/2}|\mathbf{a}|^2} \tag{31}$$

and

$$q_m r=\pi . \tag{32}$$

Using Eq. (28), the Raman scattering for $n=$TA phonon is rewritten as

$$I_{\mathrm{TA}}(\omega)\sim C_{\mathrm{TA}}^2(\omega)\frac{2S(2S+1)}{3}\frac{\chi_{zz}}{\chi_0}\frac{1}{1-e^{-\beta\hbar\omega}}\frac{2\Omega}{\pi^2 r^2}\times\int_0^{\omega_m}d\hat{\omega}_{\mathrm{TA}}(\mathbf{q})\left[\frac{1}{\hat{\omega}_{\mathrm{TA}}(\mathbf{q})}\left[\frac{\Gamma_{\mathrm{TA}}(\mathbf{q})}{[\omega-\hat{\omega}_{\mathrm{TA}}(\mathbf{q})]^2+\Gamma_{\mathrm{TA}}^2(\mathbf{q})}-\frac{\Gamma_{\mathrm{TA}}(\mathbf{q})}{[\omega+\hat{\omega}_{\mathrm{TA}}(\mathbf{q})]^2+\Gamma_{\mathrm{TA}}^2(\mathbf{q})}\right]\frac{\sin^{-1}[\hat{\omega}_{\mathrm{TA}}(\mathbf{q})/\omega_m]}{[\omega_m^2-\hat{\omega}_{\mathrm{TA}}^2(\mathbf{q})]^{1/2}}\right] . \tag{33}$$

Here Ω is the surface area of the crystal. Moreover, we assume that[35]

$$\Gamma_{\mathrm{TA}}(\mathbf{q})=\frac{\Gamma_0}{100}\hat{\omega}_{\mathrm{TA}}(\mathbf{q}) . \tag{34}$$

Using appropriate parameters of ω_m, Γ_0, and C_0, which is given by

$$C_0^2=C_{\mathrm{TA}}^2(\omega)\frac{2S(2S+1)}{3}\frac{\chi_{zz}}{\chi_0}\frac{2\Omega}{\pi^2 r^2} , \tag{35}$$

and is assumed to be independent of ω, we fit Eq. (33) with our Raman spectra, as shown in Fig. 7. The agreement between the theoretical and experimental spectra is quite good except for the low-frequency region. The ob-

tained parameters are shown in Figs. 8 and 9. It should be noted that the intensity of the low-frequency spectrum below 30 cm^{-1} is weaker than the theoretical one above 148 K. In particular at 294 K the observed low-frequency spectrum is much weaker than the theoretical one. This leads us the conclusion that C_0^2 has a strong frequency dependence in the low-frequency region, which decreases with decreasing ω.

We plotted $I(\omega)/[n(\omega)+1]$ which was observed at $\omega=+10$ cm^{-1} in the present experiment and which is approximately proportional to C_0^2 observed at $\omega=+10$ cm^{-1}, in Fig. 8, too. It has stronger temperature dependence than C_0^2 and shows a maximum at T_N, which suggests that there exists another scattering process of light in the low-frequency region.

The square of coupling constant is proportional to the magnetic susceptibility which is written as Eq. (26). If we set $[J(\mathbf{t}_2^*/2)-J(\mathbf{q})]/J(\mathbf{t}_2^*/2)=0.25$, we obtained a dashed curve in Fig. 8, and it matches well with our data of C_0^2.

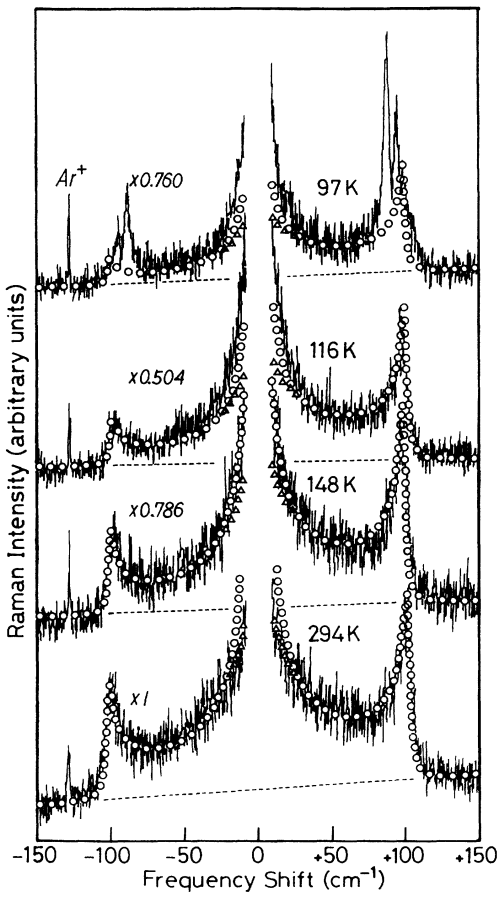

FIG. 7. Comparison between the experimental Raman spectra and the calculated Raman spectra due to the spin-disorder-induced Raman scattering from the TA phonon. Open circles denote the Raman spectra calculated by assuming that C_0^2 of Eq. (35) is independent of ω and triangles those calculated by taking into account the ω dependence of C_0^2 below 30 cm^{-1} as shown in Fig. 10. The dashed lines show the backgrounds in the calculation. Ar^+ means a plasma line of an Ar^+ laser.

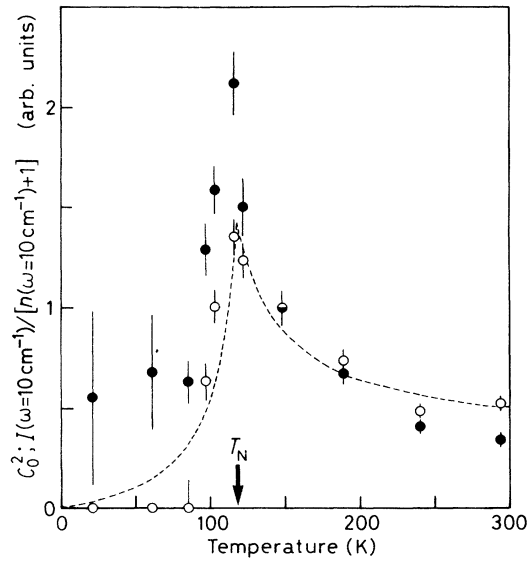

FIG. 8. Temperature dependence of C_0^2 used in the calculation and $I(\omega)/[n(\omega)+1]$ observed at $\omega=+10$ cm^{-1}. We set them unit at 148 K. A dotted curve denotes the Ornstein-Zernike form of Eqs. (26), (27a), and (27b) with $[J(\mathbf{t}_2^*/2)-J(\mathbf{q})]/J(\mathbf{t}_2^*/2)=0.25$.

VII. MAGNETIC CRITICAL SCATTERING

$I(\omega=+10\ cm^{-1})/[n(\omega=+10\ cm^{-1})+1]$ is approximately proportional to C_0^2 observed at $+10$ cm^{-1}, where $n(\omega)$ is the Bose factor, and it seems to diverge at T_N. We consider the central component to be due to the magnetic critical scattering in addition to the spin-disorder-induced Raman scattering from the TA phonon.

In Fig. 7, the intensity of the low-frequency spectrum observed at 294 K is weaker than the calculated one due to the spin-disorder-induced Raman scattering from the

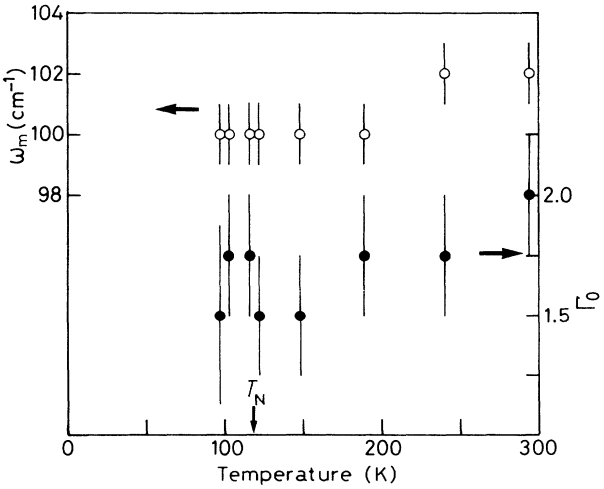

FIG. 9. Temperature dependence of ω_m and Γ_0 used in the calculation.

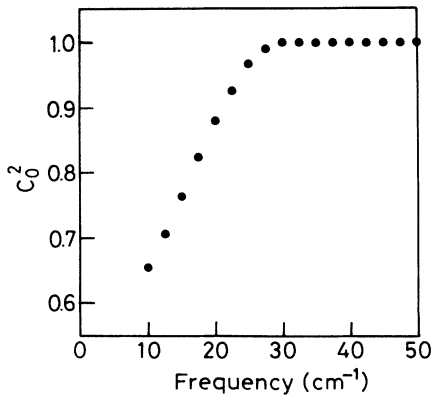

FIG. 10. The ω dependence of C_0^2. It was set unit above 30 cm^{-1} and obtained assuming that the theoretical curve of Eq. (33) agrees with the experimental Raman spectrum at 294 K.

TA phonon. This difference comes from neglect of the $\mathbf{q}$ dependence of $C_{TA}^2(\mathbf{q})$ and $\chi_{zz}(\mathbf{q})$. This neglect is not appropriate in the small-$|\mathbf{q}|$ region, since the electron-phonon interaction of TA phonon is strongly $\mathbf{q}$ dependent particularly in the small-$|\mathbf{q}|$ region and it decreases as q becomes small.[37] On the other hand, $\chi_{zz}(\mathbf{q})$ increases abruptly around $\mathbf{q}=\mathbf{t}_2^*/2$ but its effect probably does not contribute to the ω dependence of C_0^2, as will be discussed later. We believe that the whole spectrum of the broad band observed at 294 K originates from the spin-disorder-induced phonon Raman scattering and the magnetic critical scattering does not contribute to it, because the temperature is far above the Néel temperature. Fitting the theoretical spectrum with the experimental one at 294 K gives us C_0^2 as a function of ω, as shown in Fig. 10. Here we set C_0^2 above 30 cm^{-1} unit. We think that the ω dependence of C_0^2 does not change when we decrease temperature. The triangles in Fig. 7 denote the theoretical spin-disorder-induced phonon Raman spectra below 30 cm^{-1}, when we calculated them taking into account the ω dependence of C_0^2. Figure 11 shows the differences between the theoretical and experimental spectra. Near the Néel temperature the quasielastic scattering due to the magnetic critical scattering is enhanced.

In the magnetic materials, the critical scattering has been often observed by inelastic-neutron-scattering experiments. The magnetic critical scattering by light also has been studied theoretically by Moriya,[38] L'vov,[39] and Halley.[40] But it has never been observed experimentally in the magnetic system by light scattering, as far as we know.

Moriya[38] reported that it is impossible to observe the critical scattering in the paramagnetic phase of the antiferromagnets when the scattering vector $\mathbf{q}_0$ is much far from the antiferromagnetic vector, since $\mathbf{q}_0$ is nearly

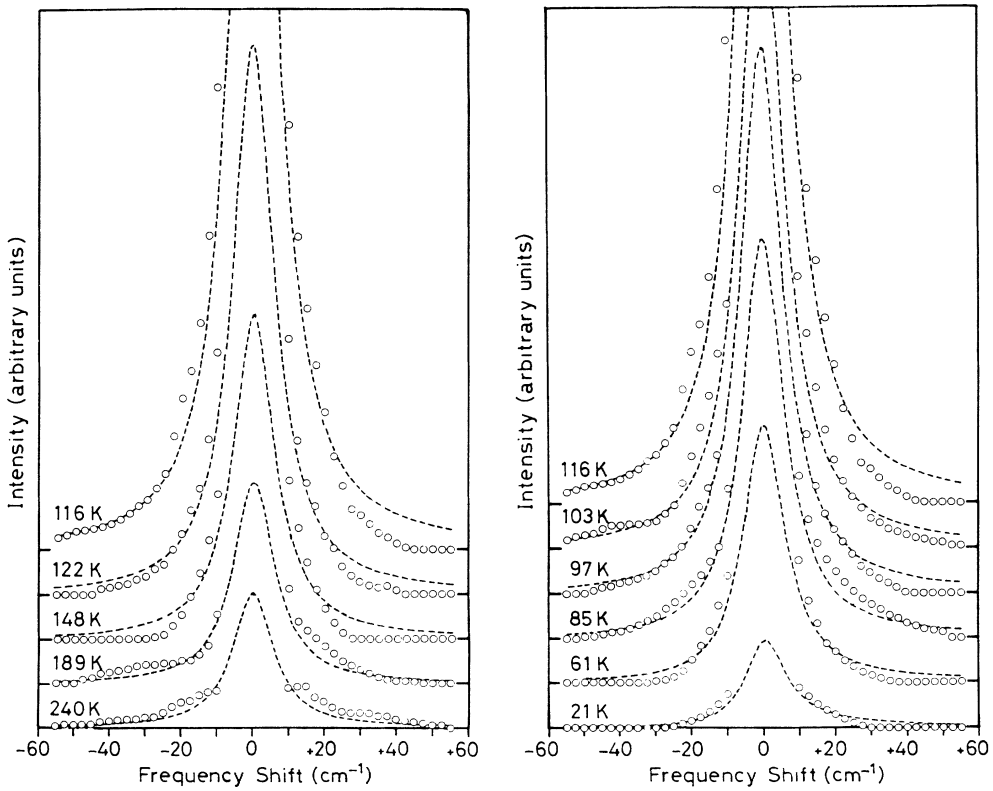

FIG. 11. Magnetic critical scattering in $FePS_3$. Open circles were obtained after subtracting the theoretical curves which were calculated by taking into account the ω dependence of C_0^2 from the experimental Raman spectra. Dotted curves show the theoretical curves obtained by Eq. (36) above T_N and by Eq. (38) below T_N under the assumption that $D_T=D_\parallel$.

equal to zero in the light scattering. But Halley[40] took into consideration the fluctuations of the energy density $E(\mathbf{q};t)$ in addition to those of the magnetization and calculated the critical scattering by hydrodynamic model of spins. At $T>T_N$, only the fluctuations of the energy density give a nonzero contribution to the critical scattering in the antiferromagnets. Then the critical scattering is given as

$$I(\omega)=\frac{\gamma}{2\pi}\int_{-\infty}^{+\infty}dt\, e^{-i\omega t}\langle E(\mathbf{q}_0;t)E^*(-\mathbf{q}_0;0)\rangle$$
$$=\frac{\gamma}{1-e^{-\beta\hbar\omega}}\frac{1}{\pi}\frac{C_T T D_T q_0^2\omega}{\omega^2+(D_T q_0^2)^2}\ , \tag{36}$$

where γ is the temperature- and ω-independent constant, C_T is the magnetic specific heat and $D_T=K_T/C_T$ when K_T is (the magnetic contribution to) the thermal conductivity. And when $\omega\sim D_T q_0^2\ll\omega_i,\omega_s$, one obtains $q_0\sim q_i\sin(\theta/2)$, where θ is the scattering angle of the light and q_i is the wave vector of the incident light, although we have assumed that $q_0=0$ in the previous discussion. When $\beta\hbar\omega\ll 1$, we obtain a Lorentzian line shape:

$$I(\omega)=\frac{\gamma}{\pi\hbar}\frac{C_T k_B T^2 D_T q_0^2}{\omega^2+(D_T q_0^2)^2}\ . \tag{37}$$

At $T<T_N$, we need to consider the magnetization m_z in addition to the energy density:

$$I(\omega)=\frac{\gamma}{2\pi}\int_{-\infty}^{+\infty}dt\, e^{-i\omega t}[\langle E(\mathbf{q}_0;t)E^*(-\mathbf{q}_0;0)\rangle+J^2\langle m_z(\mathbf{q}_0;t)m_z^*(-\mathbf{q}_0;0)\rangle]$$
$$=\frac{\gamma}{1-e^{-\beta\hbar\omega}}\frac{1}{\pi}\left[\frac{C_T T D_T q_0^2\omega}{\omega^2+(D_T q_0^2)^2}+J^2\frac{\chi_\parallel D_\parallel q_0^2\omega}{\omega^2+(D_\parallel q_0^2)^2}\right]. \tag{38}$$

Here $D_\parallel$ is the diffusion constant for the component of the magnetization parallel to the sublattice magnetization, $\chi_\parallel$ is the parallel susceptibility (not staggered) in units of $(g\mu_B)$, and J is the exchange.

We fitted Eqs. (36) and (38) with experimental spectra, assuming that $D_T q_0^2=7\ \text{cm}^{-1}$ at $T>T_N$ and $D_T q_0^2=D_\parallel q_0^2=7\ \text{cm}^{-1}$ at $T<T_N$ for simplicity. The dotted curves in Fig. 11 denote the theoretical spectra which are calculated using the method of least squares. The agreement is very excellent. The obtained $C_T T$ $(T>T_N)$ and $C_T T+J^2\chi_\parallel$ $(T<T_N)$ are shown in Fig. 12.

VIII. ONE-MAGNON RAMAN SCATTERING

The 122-cm^{-1} (21-K) Raman peak appears far below T_N and its frequency shifts to the high-frequency side as the temperature is decreased. The corresponding sharp peak showing the same frequency shift was also observed by infrared absorption. No other phonon peaks showing such a large frequency shift were observed by Raman-scattering and infrared-absorption measurements. We, therefore, assign it to a magnon.

It should be noted that the spin-disorder-induced phonon Raman spectrum disappears and at the same temperature the one-magnon Raman spectrum begins to emerge. Güntherodt *et al.*[26] and Silberstein[20] stated that the spin-disorder-induced phonon Raman spectrum is continuously switched to a sharp Raman line originating from the second-order process of one magnon plus one phonon in the ferromagnetic states of EuS and EuO. But we observed no such continuous switching from the broad band due to the spin-disorder-induced Raman scattering to a sharp peak. Although the broad band due to the spin-disorder-induced process was not observed by our infrared-absorption measurement, we observed a sharp absorption peak showing the same frequency shift as that of the Raman line. The sharp line cannot be attributed to the second-order process of one magnon plus one phonon.

Raman scattering from one magnon and two magnons have been discussed theoretically by many authors.[5,6] The Raman scattering from one magnon is derived from the fourth term in Eq. (5).[33,41]

IX. DISCUSSION

$FePS_3$ has a layered structure and its primitive unit cell is shown in Fig. 1(a). Below T_N the magnetic superstruc-

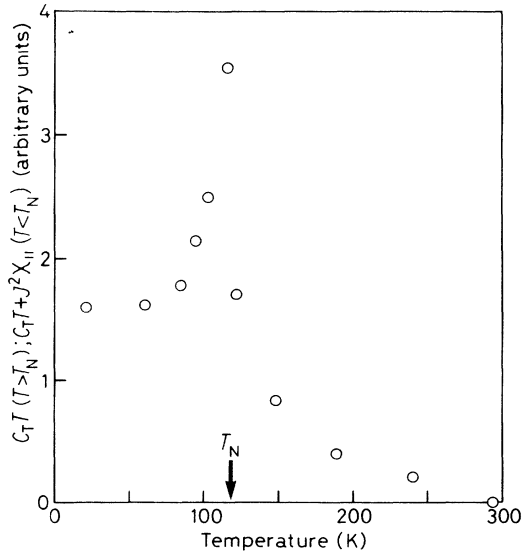

FIG. 12. Temperature dependence of $C_T T$ above T_N and $C_T T+J^2\chi_\parallel$ below T_N.

ture is formed not only along the basal plane but also along the c axis. The zone-boundary phonons at $\mathbf{q}=\mathbf{t}_2^*/2$, $\mathbf{q}=\mathbf{t}_3^*/2$, and $\mathbf{q}=\mathbf{t}_2^*/2+\mathbf{t}_3^*/2$ become Raman active in the antiferromagnetic ordered state. The Raman peaks observed at 88, 94, and 108 cm^{-1} are assigned to the zone-boundary phonons at $\mathbf{q}=\mathbf{t}_2^*/2$, because their frequencies approximately agree with the calculated ones.[36] We observed no zone-boundary phonons at $\mathbf{q}=\mathbf{t}_3^*/2$ and $\mathbf{q}=\mathbf{t}_2^*/2+\mathbf{t}_3^*/2$. It suggests that the spin-phonon interaction along the basal plane is much stronger than that perpendicular to the basal plane, reflecting the two dimensionality in the spin-phonon system. Probably it is related to the fact that the magnetostriction effect was observed only along the basal plane.[42]

The effect of two dimensionality also was observed in the spin-disorder-induced Raman scattering. The TA phonons with $q_z=0$, where q_z is perpendicular to the basal plane, participates in this scattering. The spectrum reflects two-dimensional density of states of the TA phonons.

We observed the low-frequency zone-boundary phonons which are induced by the spin ordering, and the TA phonons which are induced by the spin disorder. For the low-frequency phonons the Fe atoms vibrate, while for the high-frequency phonons they do not move and their frequencies approximately agree with those of vibrations of P_2S_6 molecule.[28] It suggests that the displacement of the magnetic ion strongly interacts with the spin of the same magnetic ion. Probably it is correlated to the magnetostriction effect.[42] However, we did not understand why only the TA phonons, in which mode atoms vibrate mainly along the z direction, contributed to this Raman scattering.

The two-dimensional density of states shows logarithmic divergences at van Hove–singularity points.[43] We adopted a one-dimensional singularity at ω_m when we calculated the spin-disorder-induced Raman spectrum. This divergence is stronger than the logarithmic one. The stronger divergence is reduced by introducing the phonon damping constant larger than the real one. The frequency of ω_m does not correspond to that of TA phonon at the M point ($\mathbf{q}=\mathbf{t}_2^*/2$), but to the K point.[36,44] The phonon at the M point was observed at 108 cm^{-1} by the spin-ordering-induced Raman scattering below T_N.

The intensity of the spin-disorder-induced phonon Raman scattering as a function of temperature shows a maximum at T_N and agrees with the Ornstein-Zernike form. This is due to an increase of the fluctuations of spin in the vicinity of the Néel temperature. As is apparent in Eqs. (25)–(27), the spin-disorder-induced Raman scattering from the TA phonons near the M point is expected to be strongly enhanced in the vicinity of T_N. However the density of states terminates at the frequency of TA phonon at the M point and the phonons near the M point do not mainly contribute to the spin-disorder-induced phonon Raman spectrum. We, therefore, think that the assumption that $[J(\mathbf{t}_2^*/2)-J(\mathbf{q})]/J(\mathbf{t}_2^*/2)$ is independent of $\mathbf{q}$ is quite good.

The three-dimensional phonon density of state is proportional to ω^2 near $\omega=0$, while the two-dimensional one is proportional to ω. In the present case the spin-disorder-induced phonon Raman scattering is written as $I_{TA}(\omega)\propto|\omega|^{-1}$ near $\omega=0$ using Eq. (33) when $k_BT\gg\hbar\omega$, which reflects the two-dimensional property. Our experimental result showed a divergence near $\omega=0$ at high temperatures. This is mainly due to the two-dimensional nature.

The intensity of the spin-disorder-induced Raman scattering near $\omega=0$ has approximately temperature dependence of $n(\omega)\sim T$. But we observed that the observed quasielastic component abruptly increased as the temperature was decreased from 294 K to T_N and showed a maximum at T_N. We cannot do without the light-scattering process of magnetic critical scattering. In particular, the quasielastic component comes mainly from the magnetic critical scattering in the vicinity of the Néel temperature. The magnetic critical scattering was able to be approximately described by only one Lorentzian with a damping constant. In the vicinity of the Néel temperature one can see the λ-type anomaly reflecting the specific heat in Fig. 12. These facts suggest that the observed magnetic critical scattering originates mainly from the energy-density fluctuations not only above but also below T_N except for the very low temperatures. Brya and Richards[45,46] studied two-spin-fluctuation light scattering in MnF_2, NiF_2, and $RbMnF_3$. The quasielastic-scattering spectrum due to the two-spin-fluctuation scattering showed approximately a Gaussian line shape. The magnetic critical scattering observed in $FePS_3$ is apparently different from it.

It is interesting that the spin-disorder-induced Raman scattering is quenched far below T_N and at almost the same temperature the one-magnon Raman scattering begins to appear. The spin-disorder-induced phonon Raman scattering may come from the short-range fluctuations of spin rather than the long-range one. This suggests that the magnon picture is correct in the temperature region where the short-range fluctuations are quenched.

X. CONCLUSION

We performed light-scattering measurements in the two-dimensional antiferromagnet $FePS_3$ as a probe of dynamical critical properties of spins. We observed the spin-ordering-induced Raman scattering from the zone-boundary phonons, the spin-disorder-induced Raman scattering from TA phonons throughout the Brillouin zone on the basal plane, the magnetic critical scattering, and the one-magnon Raman scattering. The integrated Raman intensity of the spin-ordering-induced phonon Raman scattering is roughly proportional to the square of the magnetic moment of the Fe^{2+} ion. The spin-disorder-induced Raman spectrum from TA phonons reflects the two-dimensional density of states. Its intensity as a function of temperature agrees well with the Ornstein-Zernike form, indicating an increase of the short-range spin fluctuations in the vicinity of the Néel temperature. The one-magnon Raman scattering was observed in the temperature region where the spin-

disorder-induced phonon Raman scattering was quenched. The quasielastic scattering due to the magnetic critical scattering was observed both above and below T_N and its intensity showed a maximum at T_N. The profile can approximately be described by a Lorentzian line shape. The magnetic critical scattering originates mainly from the energy-density fluctuations. The present experiment is the first observation of magnetic critical scattering by light.

ACKNOWLEDGMENTS

We are grateful to Dr. M. A. Kanehisa, Dr. K. Kubo, and Professor S. Takada for fruitful discussion. We also thank Dr. G. Ouvrard for providing us with $FePS_3$ samples. This work was partly supported by European Economic Community under a Stimulation Program. The Laboratoire de Physique des Solides is associé au Centre National de la Recherche Scientifique.

*Present address: Department of Physics, Faculty of Science and Technology, Sophia University, 7-1 Kioi-cho, Chiyoda-ku, Tokyo 102, Japan.

[1]R. Brec, Solid State Ion. **22**, 3 (1986).
[2]K. Kurosawa, S. Saito, and Y. Yamaguchi, J. Phys. Soc. Jpn. **52**, 3919 (1983).
[3]W. Marshall and R. D. Lowde, Rep. Prog. Phys. **31**, 705 (1971).
[4]H. Mori and K. Kawasaki, Prog. Theor. Phys. **27**, 529 (1962).
[5]W. Hayes and R. Loudon, *Scattering of Light by Crystals* (Wiley, New York, 1978), p. 239.
[6]D. J. Lockwood, in *Light Scattering in Solids III,* Vol. 51 of *Topics in Applied Physics,* edited by M. Cardona and G. Güntherodt (Springer-Verlag, Berlin, 1982), p. 59.
[7]E. F. Steigmeier and G. Harbeke, Phys. Kondens. Mater. **12**, 1 (1970).
[8]N. Suzuki and H. Kamimura, Solid State Commun. **11**, 1603 (1972); J. Phys. Soc. Jpn. **35**, 985 (1973).
[9]N. Koshizuka, Y. Yokoyama, and T. Tsushima, Solid State Commun. **18**, 1333 (1976); **23**, 967 (1977).
[10]M. Iliev, G. Güntherodt, and H. Pink, Solid State Commun. **27**, 863 (1978).
[11]M. N. Iliev, E. Ansatassakis, and T. Arai, Phys. Status Solidi B **86**, 717 (1978).
[12]N. Koshizuka, S. Ushioda, and T. Tsushima, Phys. Rev. B **21**, 1316 (1980).
[13]G. Güntherodt, J. Magn. Magn. Mater. **11**, 394 (1979).
[14]S. A. Safran, J. Phys. (Paris) Colloq. **41**, C5-223 (1980).
[15]A. Mauger and C. Godart, Phys. Rep. **141**, 51 (1986).
[16]J. C. Tsang, M. C. Dresselhaus, R. L. Aggarwal, and T. B. Reed, Phys. Rev. B **9**, 984 (1974).
[17]J. C. Tsang, M. S. Dresselhaus, R. L. Aggarwal, and T. B. Reed, Phys. Rev. B **9**, 997 (1974).
[18]R. P. Silberstein, L. E. Schmutz, V. J. Tekippe, M. S. Dresselhaus, and R. L. Aggarwal, Solid State Commun. **18**, 1173 (1976).
[19]R. P. Silberstein, V. J. Tekippe, and M. S. Dresselhaus, Phys. Rev. B **16**, 2728 (1977).
[20]R. P. Silberstein, Phys. Rev. B **22**, 4791 (1980).
[21]L. E. Schmutz, G. Dresselhaus, and M. S. Dresselhaus, J. Magn. Magn. Mater. **11**, 412 (1979).
[22]S. A. Safran, G. Dresselhaus, and B. Lax, Phys. Rev. B **16**, 2749 (1977).
[23]S. A. Safran, R. P. Silberstein, G. Dresselhaus, and B. Lax, Solid State Commun. **29**, 339 (1979).
[24]S. A. Safran, G. Dresselhaus, R. P. Silberstein, and B. Lax, J. Magn. Magn. Mater. **11**, 403 (1979).
[25]G. Güntherodt, W. Bauhofer, and G. Benedek, Phys. Rev. Lett. **43**, 1427 (1979).
[26]G. Güntherodt, R. Merlin, and P. Grünberg, Phys. Rev. B **20**, 2834 (1979).
[27]M. Scagliotti, M. Jouanne, M. Balkanski, and G. Ouvrard, Solid State Commun. **54**, 291 (1985).
[28]M. Scagliotti, M. Jouanne, M. Balkanski, G. Ouvrard, and G. Benedek, Phys. Rev. B **35**, 7097 (1987).
[29]M. Balkanski, M. Jouanne, G. Ouvrard, and M. Scagliotti, J. Phys. C **20**, 4397 (1987).
[30]N. Suzuki, J. Phys. Soc. Jpn. **40**, 1223 (1976).
[31]Y. Ousaka, O. Sakai, and M. Tachiki, Solid State Commun. **23**, 589 (1977); J. Phys. Soc. Jpn. **48**, 1269 (1980); **52**, 1034 (1983); O. Sakai and M. Tachiki, J. Phys. Chem. Solids **39**, 269 (1978).
[32]R. Zeyer and W. Kress, Phys. Rev. B **20**, 2850 (1979).
[33]T. Moriya, J. Phys. Soc. Jpn. **23**, 490 (1967).
[34]R. Merlin, R. Zeyher, and G. Güntherodt, Phys. Rev. Lett. **39**, 1215 (1977).
[35]A. A. Maradudin and A. E. Fein, Phys. Rev. **128**, 2589 (1962).
[36]M. Bernasconi, G. L. Marra, G. Benedek, L. Miglio, M. Jouanne, C. Julien, M. Scagliotti, and M. Balkanski, Phys. Rev. B **38**, 12 089 (1988).
[37]R. Loudon, Proc. R. Soc. London Ser. A **275**, 218 (1963).
[38]T. Moriya, J. Appl. Phys. **39**, 1042 (1968).
[39]V. S. L'vov, Fiz. Tverd. Tela (Leningrad) **10**, 451 (1968) [Sov. Phys. Solid State **10**, 354 (1968)].
[40]J. W. Halley, Phys. Rev. Lett. **41**, 1605 (1978).
[41]R. Loudon, J. Phys. C **3**, 872 (1970).
[42]P. Jernberg, S. Bjarman, and R. Wäppling, J. Magn. Magn. Mater. **46**, 178 (1984).
[43]B. L. Evans, in *Optical and Electrical Properties,* Vol. 4 of *Physics and Chemistry of Materials with Layered Structures,* edited by P. A. Lee (D. Reidel, Dordrecht, 1976), p. 1.
[44]G. Benedek and A. Frey, Phys. Rev. B **21**, 2482 (1980).
[45]W. J. Brya and P. M. Richards, Phys. Rev. B **9**, 2244 (1974).
[46]P. M. Richards and W. J. Brya, Phys. Rev. B **9**, 3044 (1974).